

# Oscillatory clusterings in compartmentalized granular systems

## Feature Article

Meiying Hou\*, Yinchang Li, Rui Liu, Yin Zhang, and Kunquan Lu

Beijing National Laboratory for Condensed Matter Physics, Institute of Physics, Chinese Academy of Sciences, Beijing 100190, P. R. China

Received 2 August 2010, revised 27 September 2010, accepted 28 September 2010

Published online 1 November 2010

**Keywords** dissipation, flux model, granular systems, nonlinear dynamics

\* Corresponding author: e-mail mayhou@aphy.iphy.ac.cn, Phone: +86-10-82649089, Fax: +86-10-82640224

A review is given of our previous work on the clustering, especially the oscillatory clustering for shaken fluidized granular matter in connected compartments, as examples for pattern formation and bifurcations in far from equilibrium systems. Flux model is presented and discussed for mono-disperse and bi-disperse granular systems. Comparison of the flux model with simulation results is given. They show reasonably well agreements. Besides the homogeneous (HOM), segregation (SEG), and oscillatory (OSC) states, two new stationary states (d-OSC and s-HOM) in the bi-disperse granular system are predicted by

our simulation. In our recent work these two new states are observed experimentally, and their flow diagrams are obtained based on the flux model, which shows qualitative agreement with the experimental results. Discussions of variations of the above system are also given, such as adding an asymmetric structure, changing the number of compartments from two to three, and adding more than two types of particles. This compartmentalized fluidized granular system turns out to be a good model system for studying nonlinear dynamics and pattern formation of far from equilibrium systems.

© 2010 WILEY-VCH Verlag GmbH & Co. KGaA, Weinheim

**1 Introduction** Pattern formation is one of the important features of systems far from equilibrium [1–5]. As a non-equilibrium system, patterns in shaken fluidized granular gas systems have caught much attention of physicists in recent years [6–14]. Such a system has emerged to be important test bed to investigate the applicability of dissipative kinetic theory in nonlinear dynamics and bifurcation theory.

Clustering is one of the patterns most commonly observed in fluidized granular systems [15–20]. In such systems, the clustering arises from the intrinsic inelastic collisions between particles. The particles collide more frequently in a region slightly denser than the others, and hence more energy is dissipated in this dense region. This results in the formation of a cluster of slowly moving particles, while relatively dilute regions are depleted, where only a few rapid particles remain.

This clustering process can be clearly viewed in a setup with two connected compartments [21], where vertical shaking spontaneously leads to one well-filled and one nearly empty compartment. This clustering behavior demonstrates the suppositive “Maxwell’s demon” experiment in which the energy dissipation between particles acts

as the demon to preferentially let particles pass only in one direction to cluster in one of the compartments [22].

More interesting clustering patterns can be found when the particles contain a mixture of bi-disperse grains which are different in size, mass, or coefficient of restitution. Such a mixture shows competitive clustering behavior [23, 24]. By tuning the shaking strength, the clustering can be directed either toward the compartment initially containing mainly the small particles, or to the one containing mainly the large particles. This kind of segregation (SEG) clustering behavior can also be found in  $N$  connected compartments, for example in three connected compartments it is found that for sufficiently strong shaking the granular gas is equipartitioned, but for lower shaking intensity the gas will cluster in one compartment [25–28].

As a nonlinear dynamical system, it is expected that oscillatory (OSC) clustering shall be happening in such a two-compartment bi-disperse granular system. Simulations by Costantini et al. [29, 30] and Lambiotte et al. [31] in 2005 demonstrated the existence of the so-called “granular clock.” This OSC clustering was soon experimentally observed by Miao et al. [32] in a compartmentalized mixture of millets and mung beans, and then this granular clock

© 2010 WILEY-VCH Verlag GmbH & Co. KGaA, Weinheim

phenomenon was performed with two types of soda lime glass particles by Viridi et al. [33] and explained by considering vertical SEG effect.

In recent few years, we have studied these clustering behaviors by experiments, simulations, and modeling. Experimentally we observed the OSC clustering in a bi-disperse system with grains of the same size, but of different masses; by measuring the oscillation period and amplitude [34, 35] we verify that the transition from SEG state to OSC state is an infinite-period bifurcation, and from OSC state to homogeneous (HOM) state is a supercritical Hopf bifurcation. By molecular dynamics simulation, we found two new stationary OSC states: a degenerate oscillation (d-OSC) state and a state with large particles segregated and small particles homogeneously distributed (s-HOM) [36], which have been verified in our recent experiments [37]. We have obtained flow diagrams of the states mentioned above based on a flux model modified from works by Mikkelsen et al. [23, 24]. The transition from d-OSC state to oscillation state demonstrates a homoclinic gluing bifurcation [37]. A comparison of simulation with the flux model was performed to quantitatively verify the validity of the flux model.

In this paper, we will first review the experimentally observed patterns in compartmentalized granular gas systems and then introduce the flux model that we have adopted, which reasonably well explains the observed clustering behavior. In the final section a discussion is presented of some variations of the compartmentalized structure, such as introducing asymmetric settings for imperfect bifurcation, changing the number of compartments, and adding more than two types of particles in the system. At the end, some final remarks conclude the paper.

**2 Experimental observation** The experimental setup consists a container made of two identical compartments, which are connected by a narrow opening at the wall in between the compartments, as is shown in Fig. 1. The setup is driven by a shaker connected to the bottom of the container. Gaining kinetic energy by colliding with the driving bottom plate, particles may jump from one compartment to the other through the opening.

When a number of particles are added randomly to this two-compartments system, depending on the shaking strength, particles will eventually either equally distribute in the two compartments, or cluster in one of the compartments. At higher shaking strength, particles are able to freely jump through the wall opening and equally distribute in the two compartments. As the strength goes lower, particles in the compartment with higher number density will encounter more inelastic collisions, which further reduce the granular temperature in this compartment, and more particles from the other compartment will flow into this compartment. Finally, the system settles at an asymmetric distribution state with dilute phase in one compartment and dense phase in the other. This spontaneous symmetry-breaking phenomenon is known as Maxwell's demon in the granular gas system, which was first observed in 1996 by

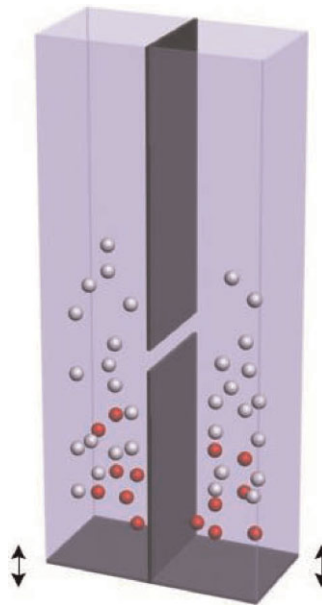


**Figure 1** (online colour at: [www.pss-a.com](http://www.pss-a.com)) Sketch of a typical two-compartment system. Two identical compartments are connected by a slit at a certain height.

Schlichting and Nordmeier [21] and successfully explained by a flux model derived by Eggers [22] in 1999.

In the mono-disperse granular gas, particles will always preferentially cluster in the compartment where more particles are initially placed. In a two species system, the coupling between the two species will lead to a competitive clustering behavior (as shown in Fig. 2). The velocity of a large or heavy particle when colliding with a smaller or lighter particle will be reduced due to conservation of momentum, while the smaller or lighter particle will gain velocity after such a collision. A system starts from the same

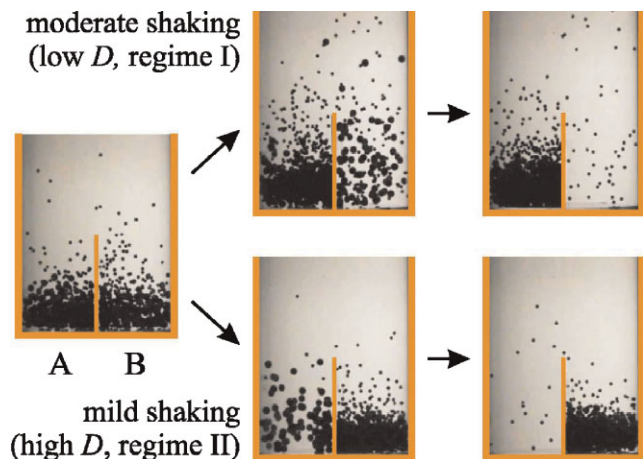


**Figure 2** (online colour at: [www.pss-a.com](http://www.pss-a.com)) Competitive clustering experiment in bi-disperse granular gases [23, 24]. With moderate shaking strength, cluster is formed in compartment A, which initially contains more large particles. At a lower shaking strength, particles cluster in the compartment initially with more small particles (compartment B).

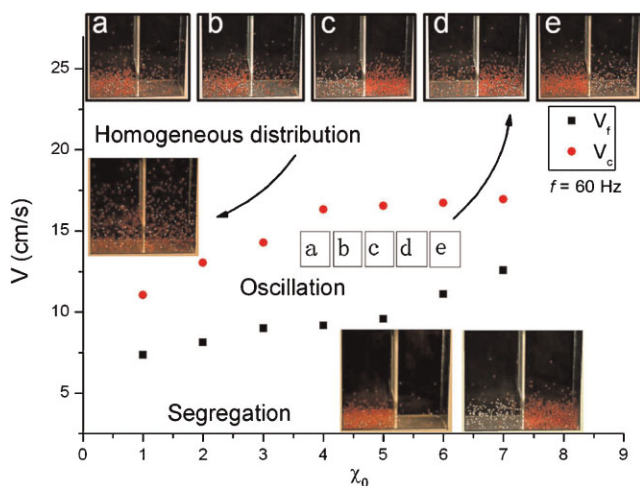


**Figure 3** (online colour at: [www.pss-a.com](http://www.pss-a.com)) OSC clustering observed in Ref. [34]. Phase diagram shows the HOM, OSC, and SEG states for different shaking velocities  $v$  and number ratios  $\chi_0$ . A full cycle of the oscillation is shown in snapshots (a)–(e).

initial state, say, more large balls and less small ones in compartment (A); particles will always cluster in the compartment A at some moderate driving strength, and cluster in the compartment B at a lower driving strength [23, 24].

In a two species system not only competitive clustering is observed, cyclic distribution among the two compartments, the granular clock phenomenon, has also been predicted by simulations [29–31, 36] and observed by experiments [32–34, 39]. This periodic distribution of bi-disperse grains in the two compartments shall not be solely explained by the Brazil nut effect (BNE) or the reverse BNE (RBNE) of vertical SEG as discussed in some previous papers [31–33].

In our experiment, an OSC state is observed in two species with the same size but different masses (Fig. 3) [34]. In the experiment, same-size glass beads and steel balls with a number ratio  $\chi_0$  ranging from 7:1 to 1:1 are filled in these two compartments. In this system particles gain energy through the shaker. It is found experimentally that the shaker's maximum shaking velocity  $v$  is a controlling parameter to the clustering behavior. At a fixed  $\chi_0$ , when the shaking velocity  $v$  is lower than a transition velocity  $v_f$ , the system is in a segregated state similar to what is observed in Refs. [23, 24]. As the shaking velocity  $v$  is within a range of two critical velocities  $v_c > v > v_f$ , particles will periodically distribute in these two compartments. As  $v$  goes higher than another transition velocity  $v_c$ , particles will homogeneously distribute in both compartments. The phase diagram is shown in Fig. 3. The OSC cycle is shown in Figs. 3(a)–(e): particles at first cluster in the left compartment [Fig. 3(a)]. Heavy particles are more likely to stay near the bottom and transfer energy to the lighter ones via collision. Those lighter particles lifted up by the heavy ones are able to go through the wall opening. With less or no help from heavy particles, they cool down and cluster in the other compartment

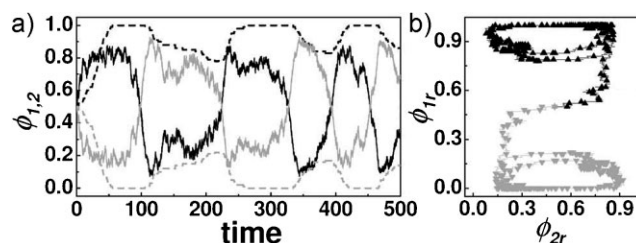


**Figure 4** (a) Oscillatory curves of the d-OSC state [ $\phi_{i\zeta} \equiv N_{i\zeta}/N_{i0}$ , where  $N_{i\zeta}$  is the particle number of species  $i$  in compartment  $\zeta$  and  $N_{i0}$  is the total number of species  $i$ ,  $i = 1$  (2) for light (heavy) particles,  $\zeta = 1$  (r) for left (right) compartment; dark solid lines indicate  $\phi_{1l}$ , gray solid lines  $\phi_{1r}$ , dark dashed lines  $\phi_{2l}$ , and gray dashed lines  $\phi_{2r}$ ], and (b) the corresponding phase orbit with two possible branches [36].

[Figs. 3(b)–(c)]. Once most of the light particles emigrate, the heavy ones are able to follow the lighter ones to jump through the opening [Figs. 3(c)–(d)]. The same cycle will repeat to let particles jump from the other compartment back to the original one [Figs. 3(d)–(e)].

The oscillation amplitude and period at a certain driving velocity  $v$  near the transition point are studied, which indicate that the transition from HOM state to OSC state is a supercritical Hopf bifurcation and the transition from SEG state to OSC state is via an infinite-period bifurcation (as shown in the following paragraph).

As the number of heavy particles is increased, a new OSC state [degenerate OSC (d-OSC) state] is found by numerical simulation [36] (Fig. 4) and then observed experimentally [37] (Fig. 5). In the simulation, event-driven algorithm for 3D systems is used. Particles are considered as perfect rigid spheres that deformations during collisions are ignored. Particle–particle and particle–boundary collisions are considered as instantaneous events. Between the two events the particles move freely keeping parabolic paths under gravitational acceleration  $g$ . At an event of collision

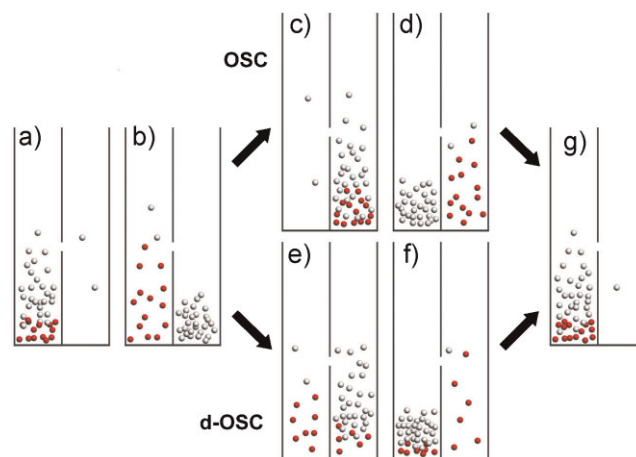


**Figure 5** (online colour at: [www.pss-a.com](http://www.pss-a.com)) Demonstration of an oscillation cycle in an OSC state: (a)–(b)–(c)–(d)–(g), and that in a d-OSC state: (a)–(b)–(e)–(f)–(g). White balls are light particles, while red (dark) ones are heavy particles.

the velocities of particles after contact are computed from the velocities just before the contact. The collisions between particle–particle and particle–boundary are considered to be inelastic with normal coefficient of restitution fixed to be 0.9. In the simulation, two species with different sizes are considered. It is found that when decreasing  $\chi_0$  to a certain value, there appears a d-OSC state, as shown in Fig. 4. In this state, the large particles mainly stay in one of the compartments with only a small number of them participating in the oscillation, while most of the small ones oscillate between the two compartments. Increasing the driving velocity, a concomitant state of the d-OSC state is observed that the small beads are homogeneously distributed (s-HOM), while the large ones show an asymmetric SEG.

An experiment is later performed to verify the existence of these two new states found in simulation. Steel particles with radius 0.75 mm and glass particles of 0.5 mm (the mass ratio reaches 9:1) are used. The total number of particles is fixed at 1000. When the portion of heavy particles  $\Phi_b$  reaches 0.35, two types of oscillation states are observed at different driving velocities. When the driving velocity is  $v = 0.15$  m/s, particles fully oscillate in two compartments [as demonstrated in Figs. 5(a)-(b)-(c)-(d)-(g)]. As the driving velocity increases to 0.19 m/s, a d-OSC state appears [Figs. 5(a)-(b)-(e)-(f)-(g)]. Initially, light particles in the presence of the heavy ones gain kinetic energy to jump from the left compartment to the right one. With no help of the heavy particles, light particles will condense in the right compartment [Figs. 5(a)-(b)]. At  $v = 0.15$  m/s, heavy particles are able to flow into the right compartment following the light ones. When all the particles are in the right compartment, the same cycle will repeat that all the particles will flow back to the left compartment and complete a full oscillation cycle [Figs. 5(c)-(d)-(g)]. As  $v$  goes higher to 0.19 m/s, for a d-OSC cycle, light particles are able to flow back to the left compartment with the help of only a small portion of the heavy particles in the right compartment [Fig. 5(e)]. With the absence of light particles in the right compartment, the small portion of heavy particles will also jump back into the left compartment [Figs. 5(f)-(g)]. This completes the oscillation cycle with only a small amount of heavy particles participating in the oscillation cycle. We call this the d-OSC state. As the driving velocity goes even higher, say 0.20 m/s, with the help of only a small portion of heavy particles participating the oscillation, the small particles are able to oscillate fast enough to be considered as homogeneously distributed. We call this s-HOM state. Based on the experimental observation, a phase diagram is plotted in Fig. 6. The controlling parameters are the driving velocity  $v$  and the percentage numbers of steel balls  $\Phi_b$ .

**3 Flux model** The experimentally observed clustering behaviors can be understood using a flux model, which describes the particle flow from one compartment to the other as a function of the shaking strength and the number of particles in the compartment. Flux models have been proposed and discussed in some previous works [22–25,

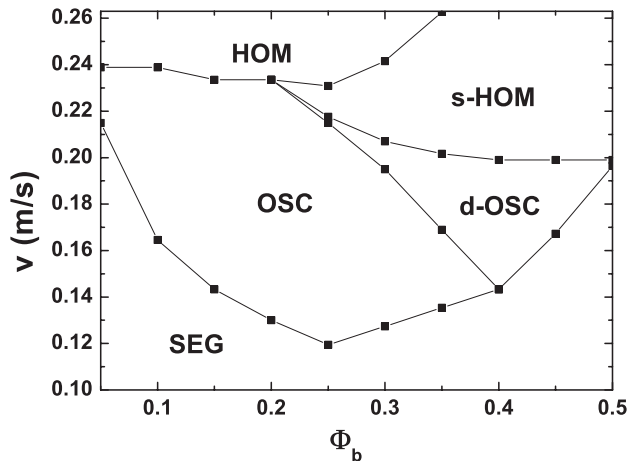


**Figure 6** Experimental confirmation of s-HOM and d-OSC state and a phase diagram obtained in  $\Phi_b$ – $v$  plane [37].

29–34, 40–44]. Following Eggers’ derivation of a mono-disperse granular gas flux function [22], Mikkelsen et al. [23, 24] have extended the model to bi-disperse granular gases. Their extended model has shown excellent agreement with experiments and simulations for N-compartment clustering and its dynamics [28]. However, in their works no OSC clustering has ever been predicted or observed. In the following subsections, we will first review their model and then extend the model to OSC states to compare with our experimental and simulation results.

**3.1 Eggers’ model** In a two-compartment mono-disperse granular gas system, the evolution of  $N$  particles in one of the compartments can be written as

$$\frac{\partial N}{\partial t} = -F(N) + F(N_0 - N). \quad (1)$$

$F(N)$  is the flux function which is assumed to be independent of time, and  $N_0$  is the total number of particles in the system. As the granular gas is dilute enough, the equation of state is written as

$$p = nk_B T, \quad (2)$$

and the momentum balance and mass conservation require

$$\frac{\partial p}{\partial z} = -mgn, \quad (3)$$

and

$$N = \int_0^{+\infty} n(z) dz. \quad (4)$$

$p$  is the pressure of the granular gas,  $n$  the granular number density,  $k_B$  the Boltzmann’s constant and is set to be 1,  $T$  the granular temperature,  $m$  the mass of the particle, and  $g$  is the gravitational acceleration. From Eqs. (2)–(4), the number

density can be solved as

$$n(z) = \frac{mgN}{\Omega k_B T} e^{-mgz/k_B T}, \quad (5)$$

where  $\Omega$  is the ground area of each compartment. The flux at location  $h$  is proportional to the product of number density and mean horizontal velocity  $\sqrt{2k_B T/\pi m}$  written as

$$F(N) = C \sqrt{\frac{m}{k_B T}} N e^{-mgh/k_B T}, \quad (6)$$

where  $C$  is equal to  $WHg/\sqrt{2\pi}\Omega$ , and  $h$  is the location of the lower edge of the opening (with an opening size  $H$ ) from the bottom. The explicit form of  $k_B T$  is written as follows [28]:

$$k_B T = \frac{\Omega^2}{16\pi(1-e^2)^2 r^4} \frac{mv^2}{N^2}, \quad (7)$$

where  $r$  is the radius of the particle,  $v$  the driving velocity and  $e$  is the normal coefficient of restitution (in this model no rotation and friction force are considered).

It is useful to study the stability of the HOM solution of Eq. (1) to investigate the essentials of the clustering phenomenon without knowing the explicit form of the flux function. The HOM distribution  $\bar{N} = N_0/2$  is a trivial solution to Eq. (1). We apply a perturbation around this solution  $N = \bar{N} + \delta N$ , and substitute it into Eq. (1), then  $\delta N$  satisfies

$$\frac{\partial \delta N}{\partial t} = -F(\bar{N} + \delta N) + F(\bar{N}). \quad (8)$$

Linearizing Eq. (8) around the HOM solution, it becomes

$$\frac{\partial \delta N}{\partial t} = -2 \frac{\partial F(N)}{\partial N} \Big|_{N=\bar{N}} \delta N. \quad (9)$$

For a stable solution near  $\bar{N}$ ,  $\frac{\partial F(N)}{\partial N} \Big|_{N=\bar{N}} > 0$  must be valid. Therefore, if HOM solution  $\bar{N}$  is located at the rising part of the flux function curve, the HOM state is a stable solution as demonstrated by the point  $a$  in Fig. 7. However, if  $\bar{N}$  is located at the declining part of the flux function, the HOM state is unstable as demonstrated by the point  $b$  in Fig. 7 in that  $b$  will evolve into two asymmetric stable states  $b_1$  and  $b_2$  under any small perturbation.

**3.2 Bi-disperse case** Similar to the mono-disperse granular gas, the evolution of  $N_i$  particles ( $i = a$  for smaller or lighter particles,  $b$  for larger or heavier particles) can be written as

$$\frac{\partial N_i}{\partial t} = -F_i(N_a, N_b) + F_i(N_{a0} - N_a, N_{b0} - N_b). \quad (10)$$

$F_i(N_a, N_b)$  is the flux function for species  $i$ , and expressed as

$$F_i(N_i) = C \sqrt{\frac{m_i}{k_B T_i}} N_i e^{-m_i g h / k_B T_i}, \quad (11)$$

where  $m_i$  and  $T_i$  refer to the mass and granular temperature of species  $i$ , respectively. For simplicity, consider the

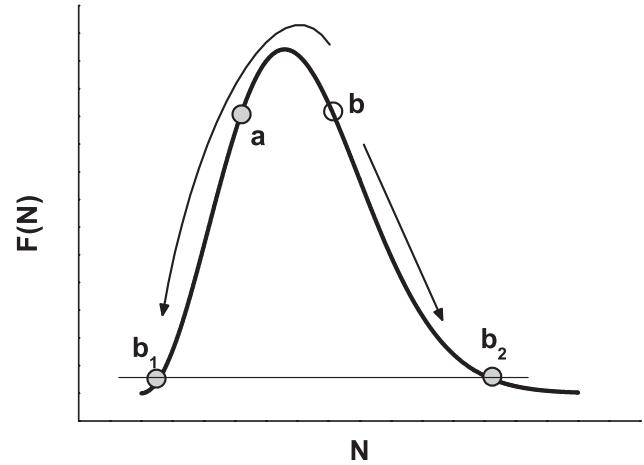


**Figure 7** Demonstration for stable and unstable HOM solutions. Gray circles present the stable solution, while hollow circle presents the unstable solution. HOM solution  $a$  is stable, and HOM unstable solution  $b$  loses its stability and changes to asymmetric stable solutions  $b_1$  and  $b_2$ .

granular temperatures of the two species to be the same:  $T_a = T_b = T$ . Under this assumption, the explicit form of the temperature can be deduced based on energy conservation:

$$k_B T = \frac{v^2 \mu}{16\pi(1-e^2)^2}. \quad (12)$$

$\mu$  is the effective mass written as

$$\mu = \left[ \frac{\Omega}{r^2} \frac{m_a N_a + m_b N_b}{\sqrt{m_a N_a^2} + \sqrt{m_b N_b^2} + m_{ab} N_a N_b} \right]^2, \quad (13)$$

where  $m_{ab}$  equals  $2\sqrt{2m_a m_b}/(m_a + m_b)$ .

In Refs. [23, 24], the particle–boundary collisions are considered elastic. In the real experiment, these collisions are always inelastic. When the system is dilute, the energy dissipation due to particle–particle collisions is comparable to that of the particle–boundary collisions. The dissipation due to particle–boundary collisions, therefore, may not be negligible. Taking into account the inelastic particle–boundary collisions, we have modified the flux function (see Ref. [37] for more details), and applied this modification to numerically solve Eq. (10); we are able to reproduce the five states mentioned in the previous section, as are shown in Fig. 8: a HOM state (which is not shown in the figure), a segregated (SEG) state, OSC state, a d-OSC state, and a small particles homogeneously distributed (s-HOM) state. The flux model can also qualitatively predict the transition from the OSC state to the SEG state when the OSC frequency goes to zero.

**3.3 Verification for flux model** Although the dynamical evolutions can be obtained theoretically, and can qualitatively match the experimental observation or

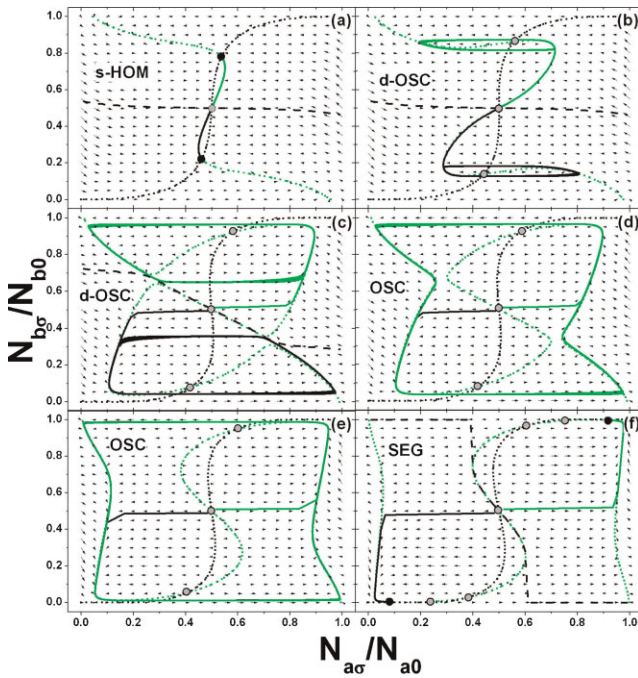


**Figure 8** (online colour at: [www.pss-a.com](http://www.pss-a.com)) Flow diagram obtained by modified flux model with same total particle numbers at different driving velocities. Evolution of system with specific initial condition (black and green solid lines); black and green dot lines correspond to  $\partial N_a/\partial t = 0$ ,  $\partial N_b/\partial t = 0$ ; dashed lines are separations between two attraction basins; the system evolution direction is shown by the vector field; gray circles represent stable fixed points, while hollow circles represent unstable fixed points [37].

simulation results, we would like to know how accurate this simplified flux model is, and which part needs improvement if the dynamical evolution comparison does not well match. In order to make a direct comparison of the model with the simulation result, we adopt a one-compartment model system (demonstrated in Fig. 9) [46].

In this simulation, we add a certain number of particles in a one-compartment cell. After the system reaches steady state, we count the number of hitting events within a slit area which centers at a vertical position  $z$  on one of the cell walls (e.g., the red area shown in Fig. 9) and average the counts over a unit time. By changing the number of particles in the container, we are able to get the flux function  $F(N_a, N_b)$  at a specific area and shaking strength.

Flux results obtained by numerical study show the same non-monotonic asymmetric feature as Eq. (6). Using  $C$  in Eq. (6) as the only fitting parameter, a comparison of the fitting result with the simulation results is shown in Fig. 10. The deviation of the two may be due to the model being oversimplified.

When another type of particles is added into the compartment, the flux functions are plotted in two contour maps (Fig. 11). The flux of light particles at first increases with the number of heavy particles, but after heavy particle number is large enough, the energy dissipation becomes large and the flux of light ones decreases with the number of

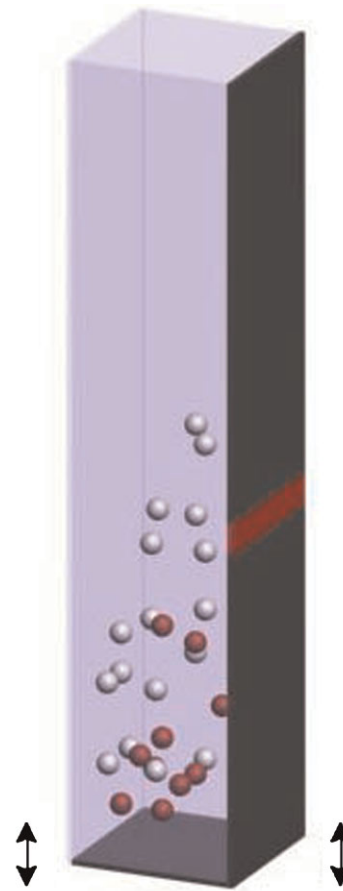


**Figure 9** (online colour at: [www.pss-a.com](http://www.pss-a.com)) Sketch of a one-compartment system. Red particles are the heavy particles, and white particles are the light ones. Red rectangle on the boundary wall represents the counting area for the flux.

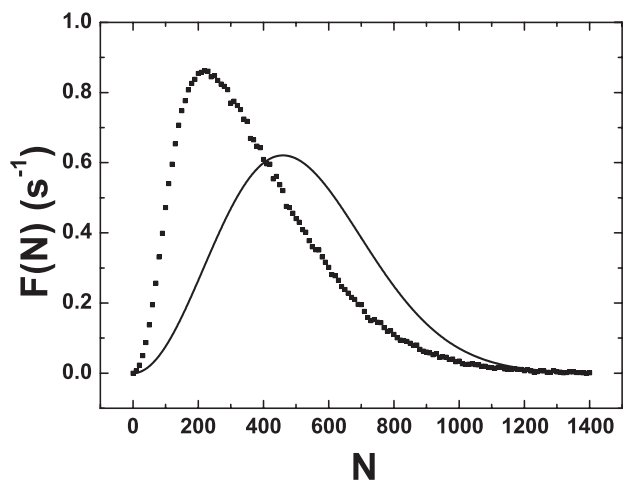


**Figure 10** Flux of mono-disperse  $F(N)$  changes with particle number  $N$ . Black points represent simulation results, solid line corresponds to the fitting results by Lohse's flux model [shown in Eq. (6)].

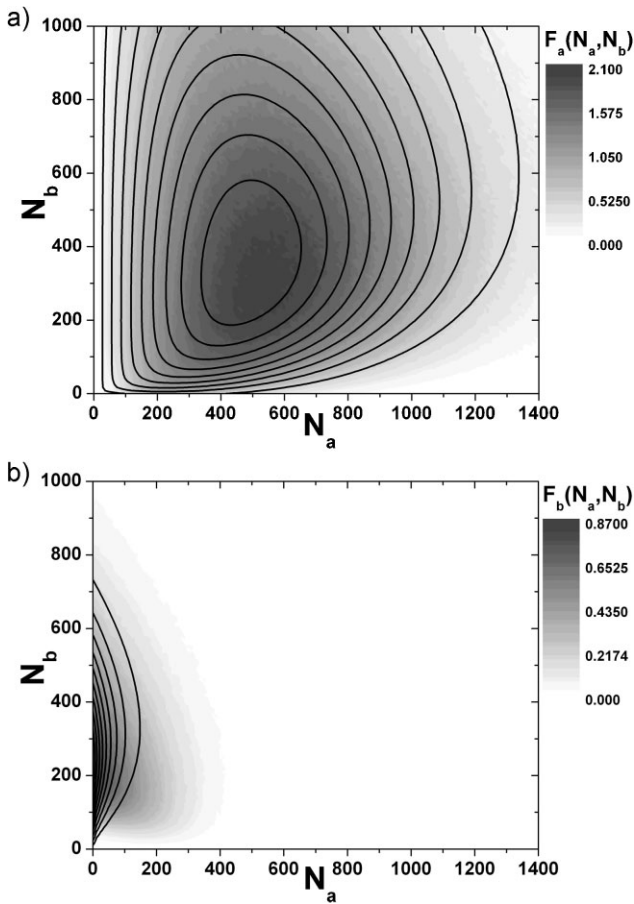


**Figure 11** Flux contour maps of bi-disperse granular gases  $F_i(N_a, N_b)$  [(a) for light particles, (b) for heavy particles]. Fitting results of modified flux model are presented by black solid lines [46].

heavy ones. The flux of heavy particles almost decreases monotonically with light ones, and this is caused by the kinetic energy lost in the transfer from heavy ones to light ones. Fitting results with Eq. (11) are shown in Fig. 11.

The flux models of mono- and bi-disperse granular gases agree qualitatively with simulation results, which is why the flux models can successfully reproduce all states observed in the experiment. The deviation due to the oversimplification of the assumptions, especially the energy equipartition between two species [38], shall be further studied by including in the flux model two granular temperatures in the future.

**3.4 Bifurcation** The transition between all the above mentioned states corresponds to different bifurcation behaviors. Investigating these bifurcation behaviors not only helps us understand the behavior of particles in compartmentalized granular systems, but also enriches our understanding of nonlinear phenomena in other systems. Here, we will briefly discuss the related bifurcation behaviors in this granular system.

For a mono-disperse gas, a transition from the HOM state to SEG state corresponds to a super-critical bifurcation.

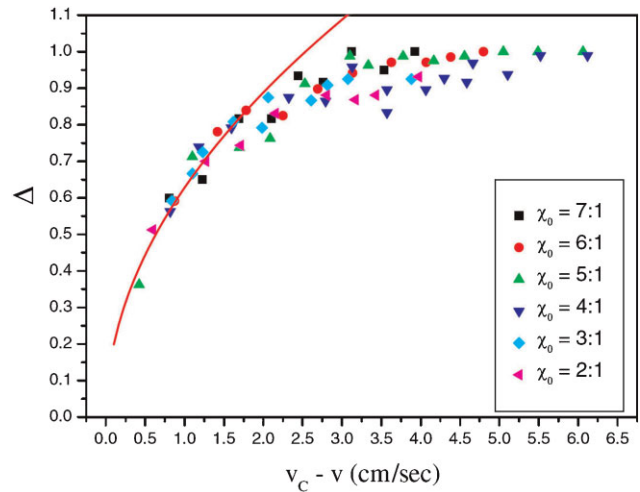


**Figure 12** (online colour at: www.pss-a.com) Variation of oscillation amplitude  $\Delta$  as a function of velocity difference  $(v_c - v)^{1/2}$  for various number ratios  $\chi_0$  (defined as  $\chi_0 = N_a/N_b$ ). The solid line is a fit of the data to the form  $\Delta \sim (v_c - v)^{1/2}$  for small  $v_c$  [34].

Recent study shows that if the curve around the peak of the flux function is symmetric, the HOM-SEG transition might be a hypercritical bifurcation generating a much stronger fluctuation than a supercritical one [47].

In bi-disperse gases, six different transitions are observed. They correspond to four different types of bifurcation behaviors. The transition from the HOM state to the s-HOM state is the same as that in HOM-SEG transition. From the study of the oscillation amplitude  $\Delta$  near the HOM-OSC transition, in that  $\Delta \sim (v_c - v)^{1/2}$  ( $v_c$  is the critical velocity) as shown in Fig. 12 which indicates the transition is supercritical Hopf bifurcation [34].

The study of the oscillation period near the SEG-OSC transition shows that the period approaches infinity at the

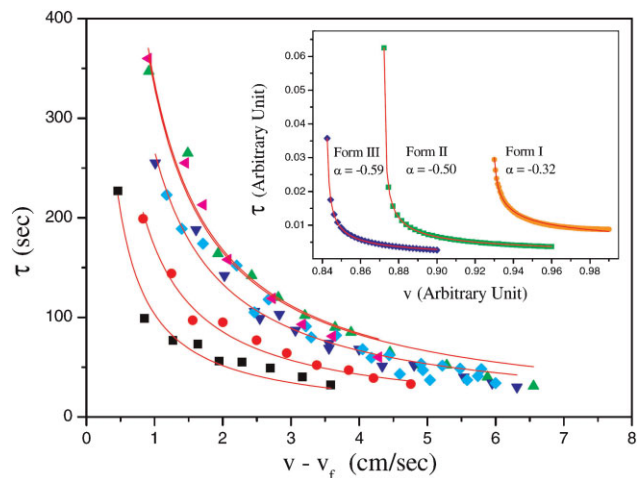


**Figure 13** (online colour at: www.pss-a.com) Variation of oscillation period  $\tau$  as a function of  $v - v_f$  ( $v_f$  is the transition velocity) measured for various  $\chi_0$ . The solid lines are fits of the data to the functional form  $(v - v_f)^{-1}$  with  $v_f$  being a fitting parameter [34].

transition point (see Fig. 13), which indicates an infinite-period bifurcation. The SEG to d-OSC transition is also found as an infinite-period bifurcation.

A global bifurcation from the d-OSC state (two limit cycles) to the OSC state (one limit cycle) is shown in Figs. 8(c)-(d). As driving velocity decreases, both limit cycles expand, and they are very close to the separatrix between attraction basins of the limit cycles [dashed line, Fig. 8(c)]. Once the limit cycle touches the separatrix, the phase portrait is connected to the saddle nodes (0.5, 0.5) and becomes a homoclinic orbit. When the driving velocity is lower, the trajectory of the limit cycle crosses the separatrix and is attracted to the other limit cycle. Because of the symmetry of the system, the two limit cycles lose their stability at the same time and glue to each other to one large limit cycle (OSC state), which corresponds to a homoclinic gluing bifurcation [Fig. 8(d)].

**4 Other configurations** In the above, the dynamical behavior of mono- and bi-disperse granular gases in two identical compartments has been well studied experimentally and theoretically. The set of flux models are able to describe behaviors of such systems. As shown in the works of van der Meer et al., interesting clustering behaviors such as “granular ratchet” and “granular fountain” [48, 49] can be obtained when extending the two-compartment system to other complicated configurations. Their works are in a mono-disperse gas system. It is reasonable to expect some interesting dynamical behaviors to emerge for bi-disperse or tri-disperse gas systems. They will not only enrich the nonlinear phenomena in a realistic system, but also give rise to some potential means for manipulating or transporting granular matters. Some primary results of our work are briefly discussed below.

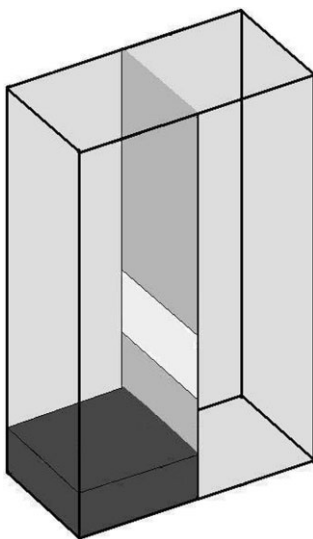


**Figure 14** Sketch of asymmetrical compartmentalized system. Dark gray cuboid presents the additional slab.

**4.1 Asymmetric structure** In order to geometrically introduce an asymmetric feature, we add a slab to the bottom of one of the compartments, say compartment A (the other being as compartment B) (The setup can be seen in Fig. 14 [51]), to see the change of the clustering behavior.

In this setup, when the driving velocity is lower than a critical value  $v_c$ , depending on the initial state and the driving strength particles can be distributed to either of the two compartments, but with a higher chance to populate compartment B, as is shown in Fig. 15. When  $v$  is higher than  $v_c$ , particles will preferentially distribute in compartment B. At even higher velocity  $v$ , particles will go asymptotically toward HOM distribution among the two compartments. This suggests that by using this configuration, we can deplete particles from compartment A to B by adjusting driving velocity.

**4.2 Bi-disperse in three compartments** It is natural to ask whether such a nonlinear system could result in a deterministic chaos behavior if more dimensions are

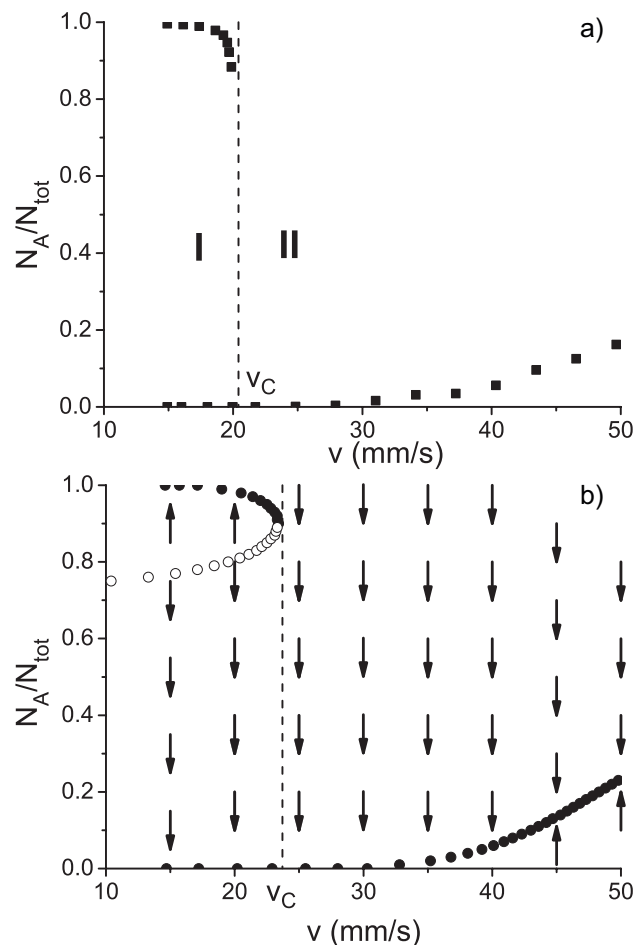


**Figure 15** Population ratio in compartment A versus driving velocity  $v$  (a) from experimental data, (b) calculated from the flux model. Solid black points represent stable state, while open circles stand for unstable solution of flux model. Arrows indicate the evolution direction of the system [51].

added into this type of system. An example is a bi-disperse granular gas in a three-compartment system. A simulation is performed using periodic boundary that each compartment is connected with the other two compartments. The evolution of the particle number  $N_i$  in compartment  $i$  can be written as

$$\begin{aligned} \frac{\partial N_{i1}}{\partial t} = & -2F_i(N_{a1}, N_{b1}) + F_i(N_{a2}, N_{b2}) \\ & + F_i(N_{a3}, N_{b3}). \end{aligned} \quad (14)$$

As the total numbers are conserved,  $N_{i1} + N_{i2} + N_{i3} = N_{i0}$ . A comparison between simulation and flux model is shown in Fig. 16 for  $N_{a0} = 1000, N_{b0} = 300$ .

A chaotic behavior is shown in Fig. 16(a), where particles randomly cluster in the three compartments and this chaotic clustering behavior is achieved through a transition from a HOM distribution state by lowering the driving velocity. Similar irregular clustering behavior has been observed experimentally in a cyclic three-compartment system [50]. But such chaotic behavior is not able to be explained by the flux model. Decreasing the shaking velocity

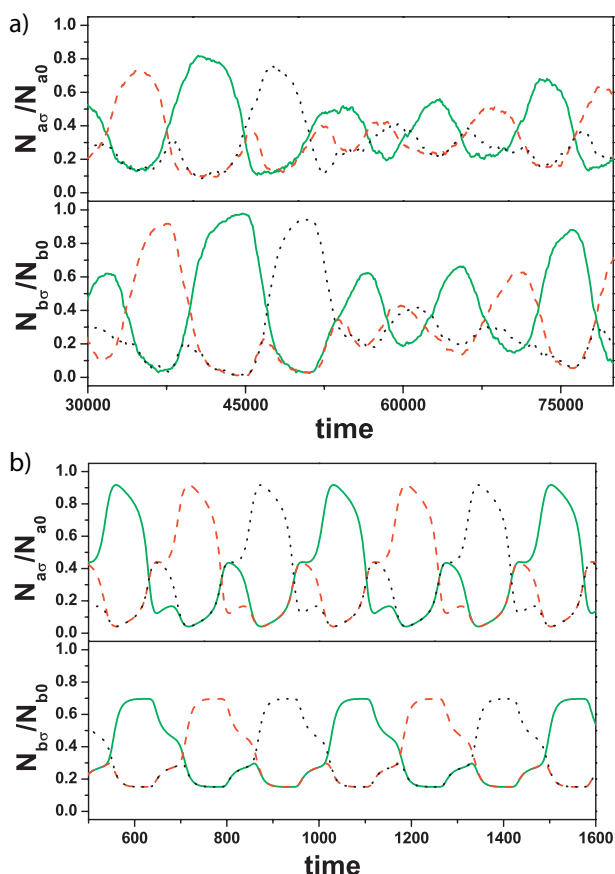


**Figure 16** (online colour at: [www.pss-a.com](http://www.pss-a.com)) Number evolution of two species (light particles in upper panel, heavy ones in lower panel) in three compartments (say, green solid lines for compartment 1, red dashed lines for compartment 2, black dot lines for compartment 3). (a) Results obtained by molecular dynamics simulation, (b) prediction by the flux model.

from the HOM state, instead of irregular clustering state, a regular directional transportation is predicted (compartment  $1 \rightarrow$  compartment  $2 \rightarrow$  compartment  $3 \rightarrow$  compartment  $1 \dots$ ), as shown in Fig. 16(b). It is easy to know such coupled differential equations has another identical-period solution except with counter direction (compartment  $3 \rightarrow$  compartment  $2 \rightarrow$  compartment  $1 \rightarrow$  compartment  $3 \dots$ ), because of the symmetry feature of the system. The disagreement between the simulation results and the prediction of flux model is eliminated by introducing a white noise term into flux model which presents the intrinsic fluctuation of system.

**4.3 Tri-disperse in two compartments** When another type of particles (only with different mass for simplicity) is added into a bi-disperse two-compartment system, the interaction between different species might become very complicated and this might lead to more interesting dynamical behaviors.

A tri-disperse granular gas simulation is performed treating the third species with smallest mass as the additive (mass ratio  $m_a : m_b : m_c$  is  $1 : 8 : 64$ ). Because of the large mass ratio, the assumption of energy equipartition becomes more unreasonable. A further flux model considering different granular temperatures is needed. Here, we just present some primary simulation results.

In Fig. 17, total numbers of species  $b$  and species  $c$  are fixed to be 600 and 200. All particles are equally distributed when there are small number of lightest particles (species  $a$ ) in the system as shown in Fig. 17(a). When more of the lightest particles are added into the system, say from 100 to 1000, species  $b$  and species  $c$  begin to oscillate in large amplitude [Fig. 17(b)]. Similar situation happens with initial number  $N_{b0} = 1000, N_{c0} = 200$ , particles asymmetrically distributed in two compartments with  $N_{a0} = 200$  [Fig. 18]. Once more lightest particles are added in ( $N_{a0} = 500$ ), the system changes from the SEG state to the OSC state. In both

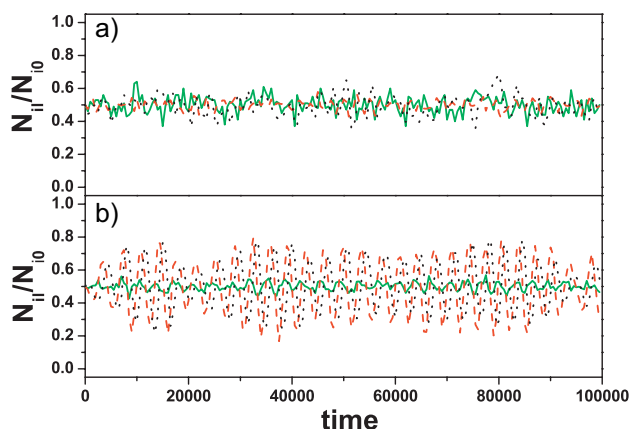


**Figure 17** (online colour at: [www.pss-a.com](http://www.pss-a.com)) Particle number evolution of three species  $i$  in left compartment (solid green lines for lightest species  $a$ , dashed red lines for heavier species  $b$ , and dot black lines for heaviest species  $c$ ). For (a)  $N_{a0} = 100, N_{b0} = 600, N_{c0} = 200$ ; (b)  $N_{a0} = 1000, N_{b0} = 600, N_{c0} = 200$ .

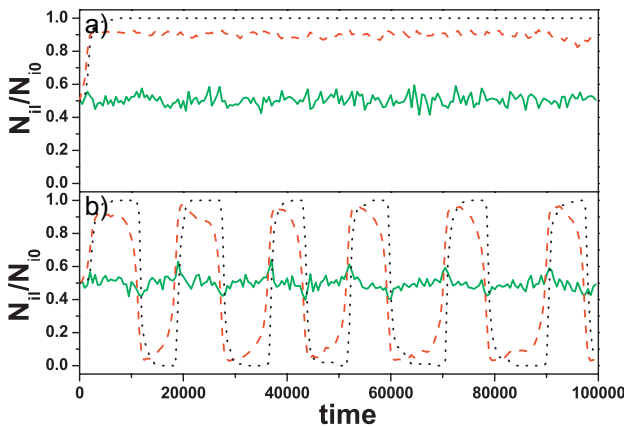


**Figure 18** (online colour at: [www.pss-a.com](http://www.pss-a.com)) Particle number evolutions for three species in two compartments. (a)  $N_{a0} = 200$ ,  $N_{b0} = 1000$ ,  $N_{c0} = 100$ ; (b)  $N_{a0} = 500$ ,  $N_{b0} = 1000$ ,  $N_{c0} = 100$ .

cases, the lightest particles are always homogeneously distributed in compartments but the presence of species  $a$  induces the system transition from stable states to OSC state. In other words, the lightest species can be seen as an oscillation catalyst.

**5 Summary** In this paper, works in clustering, especially OSC clusterings in the compartmentalized mono- and bi-disperse granular gases are reviewed. In such systems spatiotemporal ordered patterns occur due to the intrinsic dissipation and coupling between the species. A simplified flux model was used for the system. Two assumptions are made in this model: (i) the distribution of temperature is independent of the height  $z$ ; (ii) the velocity distribution is Maxwellian and isotropic. Although the temperature can be considered constant only above a certain height [22], and the velocity distribution in this driven system is non-Gaussian [45], this simple flux model seems to have the essentials capturing the clustering phenomena. We have tested the accuracy of this model by molecular simulation in a one-compartment system, and found that the simulated flux results agree reasonably well with the model. Besides the HOM, SEG and OSC states, the simulation predicts two new states, d-OSC and s-HOM clustering states. These two states are recently confirmed by our experiment and modeling works. Also bifurcation behaviors between the above states are studied both theoretically and experimentally.

Being seemingly simple and relatively well-modeled, such a compartmentalized granular gas system may be considered as a model system among others such as chemical reaction systems, fluid systems, and optical systems, for understanding the dynamics of nonlinear phenomena in far from equilibrium systems. Interesting problems such as, to characterize the system noise, to understand the effect of the noise on different clustering states, and the different bifurcations among these states. Primary results obtained in specifically designed compartments, and in a system with more than two species or two compartments, indicate that

more complicated and interesting phenomena are yet awaiting further explorations.

**Acknowledgements** This work was supported by the National Natural Science Foundation of China (grant no. 10720101074 and 10874209) and Chinese Academy of Sciences (grants no. KKCX1-YW-03 and KJCX2-YW-L08).

## References

- [1] B. Christiansen, P. Alstrom, and M. T. Levinsen, *Phys. Rev. Lett.* **68**, 2157 (1992).
- [2] M. C. Cross and P. C. Hohenberg, *Rev. Mod. Phys.* **65**, 851 (1993).
- [3] S. Edwards and S. Fauve, *J. Fluid Mech.* **278**, 123 (1994).
- [4] A. Kudrolli and J. P. Gollub, *Physica D* **97**, 133 (1996).
- [5] J. P. Gollub and J. S. Langer, *Rev. Mod. Phys.* **71**, S396 (1999).
- [6] F. Melo, P. B. Umbanhowar, and H. L. Swinney, *Phys. Rev. Lett.* **75**, 3838 (1995).
- [7] P. B. Umbanhowar, F. Melo, and H. L. Swinney, *Nature (London)* **382**, 793 (1996).
- [8] H. M. Jaeger, S. R. Nagel, and R. P. Behringer, *Rev. Mod. Phys.* **68**, 1259 (1996).
- [9] K. Liffman, G. Metcalfe, and P. Cleary, *Phys. Rev. Lett.* **79**, 4574 (1997).
- [10] G. H. Ristow, G. Strassburger, and I. Rehberg, *Phys. Rev. Lett.* **79**, 833 (1997).
- [11] J. S. Olafsen and J. S. Urbach, *Phys. Rev. Lett.* **81**, 4369 (1998).
- [12] G. H. Ristow, *Pattern Formation in Granular Materials* (Springer, New York, 2000), p. 161.
- [13] T. Shinbrot, *Nature (London)* **429**, 352 (2004).
- [14] I. S. Aranson and L. S. Tsimring, *Rev. Mod. Phys.* **78**, 641 (2006).
- [15] I. Goldhirsch and G. Zanetti, *Phys. Rev. Lett.* **70**, 1619 (1993).
- [16] S. McNamara and W. R. Young, *Phys. Rev. E* **50**, R28 (1994).
- [17] Y. Du, H. Li, and L. P. Kadanoff, *Phys. Rev. Lett.* **74**, 1268 (1995).
- [18] S. McNamara and W. Young, *Phys. Rev. E* **53**, 5089 (1996).
- [19] T. Zhou and L. P. Kadanoff, *Phys. Rev. E* **54**, 623 (1996).
- [20] E. Grossman and M. Mungan, *Phys. Rev. E* **53**, 6435 (1996).
- [21] H. J. Schlichting and V. Nordmeier, *Math. Naturwiss. Unterr.* **49**, 323 (1996).
- [22] J. Eggers, *Phys. Rev. Lett.* **83**, 5322 (1999).
- [23] R. Mikkelsen, D. van der Meer, K. van der Weele, and D. Lohse, *Phys. Rev. Lett.* **89**, 214301 (2002).
- [24] R. Mikkelsen, D. van der Meer, K. van der Weele, and D. Lohse, *Phys. Rev. E* **70**, 061307 (2004).
- [25] K. van der Weele, D. van der Meer, M. Versluis, and D. Lohse, *Europhys. Lett.* **53**, 328 (2001).
- [26] D. van der Meer, K. van der Weele, and D. Lohse, *Phys. Rev. E* **63**, 061304 (2001).
- [27] D. van der Meer, K. van der Weele, and D. Lohse, *Phys. Rev. Lett.* **88**, 174302 (2002).
- [28] D. van der Meer, K. van der Weele, P. Reimann, and D. Lohse, *J. Stat. Mech.: Theory Exp.* **P07021** (2007).
- [29] G. Costantini, D. Paolotti, C. Cattuto, and U. M. B. Marconi, *Physica A* **347**, 411 (2005).

- [30] U. M. B. Marconi, G. Costantini, and D. Paolotti, *J. Phys.: Condens. Matter* **17**, S2461 (2005).
- [31] R. Lambiotte, J. M. Salazar, and L. Brenig, *Phys. Lett. A* **343**, 224 (2005).
- [32] T. Miao, Y. Liu, F. Miao, and Q. Mu, *Chin. Sci. Bull.* **50**, 740 (2005).
- [33] S. Viridi, M. Schmick, and M. Markus, *Phys. Rev. E* **74**, 041301 (2006).
- [34] M. Hou, H. Tu, R. Liu, Y. Li, K. Lu, P. Lai, and C. K. Chan, *Phys. Rev. Lett.* **100**, 068001 (2008).
- [35] P. Lai, M. Hou, and C. Chan, *J. Phys. Soc. Jpn.* **78**, 041001 (2009).
- [36] R. Liu, Y. Li, and M. Hou, *Phys. Rev. E* **79**, 052301 (2009).
- [37] Y. Li, L. Rui, and M. Hou, to be submitted.
- [38] R. D. Wildman and D. J. Parker, *Phys. Rev. Lett.* **88**, 064301 (2002). K. Feitosa, N. Menon, *Phys. Rev. Lett.* **88**, 198301 (2002).
- [39] K. C. Chen, C. C. Li, C. H. Lin, and G. H. Guo, *Phys. Rev. E* **79**, 021307 (2009).
- [40] J. J. Brey, F. Moreno, R. García-Rojo, and M. J. Ruiz-Montero, *Phys. Rev. E* **65**, 011305 (2001).
- [41] A. Lipowski and M. Droz, *Phys. Rev. E* **65**, 031307 (2002).
- [42] F. Coppex, M. Droz, and A. Lipowski, *Phys. Rev. E* **66**, 011305 (2002).
- [43] F. Cecconi, A. Puglisi, U. M. B. Marconi, and A. Vulpiani, *Phys. Rev. Lett.* **90**, 064301 (2003).
- [44] I. Bena, F. Coppex, M. Droz, and A. Lipowski, *Phys. Rev. Lett.* **91**, 160602 (2003).
- [45] F. Rouyer and N. Menon, *Phys. Rev. Lett.* **85**, 3676 (2000). J. S. van Zon, F. C. MacKintosh, *Phys. Rev. Lett.* **93**, 038001 (2004).
- [46] Y. Li, R. Liu, and M. Hou, to be submitted.
- [47] M. Leconte and P. Evesque, *arXiv:physics* **0609204**, (2006).
- [48] D. van der Meer, P. Reimann, K. van der Weele, and D. Lohse, *Phys. Rev. Lett.* **92**, 184301 (2004).
- [49] K. van der Weele, G. Kanellopoulos, C. Tsiavos, and D. van der Meer, *Phys. Rev. E* **80**, 011305 (2009).
- [50] Y. Liu, Q. Mu, T. Miao, and J. Liao, *Europhys. Lett.* **84**, 14004 (2008).
- [51] Y. Zhang, Y. Li, R. Liu, and M. Hou, to be submitted.